# Underwater bionic whisker sensor based on triboelectric nanogenerator for passive vortex perception

Siyuan Wang [a,1], Peng Xu [a,1], Xinyu Wang [a,1], Jiaxi Zheng [b], Xiangyu Liu [a], Jianhua Liu [a], Tianyu Chen [a], Hao Wang [a], Guangming Xie [c,*], Jin Tao [d,*], Minyi Xu [a,*]

[a] *Dalian Key Lab of Marine Micro/Nano Energy and Self-powered Systems, Marine Engineering College, Dalian Maritime University, Dalian 116026, China*
[b] *Transportation Engineering College, Dalian Maritime University, Dalian 116026, China*
[c] *College of Artificial Intelligence, Nankai University, Tianjin 300350, China*
[d] *Intelligent Biomimetic Design Lab, College of Engineering, Peking University, Beijing 100871, China*

## ARTICLE INFO

## ABSTRACT

Seals, as well as other terrestrial and marine animals, utilize their whiskers as key tactile sensors to locate and track underwater wakes. Herein, an underwater bionic whisker sensor (UBWS) based on triboelectric nano-generator was designed for capturing complex stimuli produced by moving aquatic species and using the acquired signals to follow their hydrodynamic trails. The UBWS is inspired by the structural properties of seal whiskers and incorporates a free-standing triboelectric nanogenerator, which gives it ability to capture vortices passively. The design of the UBWS is fully flexible and self-powered, which eliminates the need for an external power source while retaining the capability of high sensitivity to stimuli. Moreover, the output signal's interaction with the movement parameters was highly correlated, and this principle was utilized to determine the relative motion state of an underwater moving object. Experiments demonstrated that the developed UBWS was capable of perceiving the hydrodynamic trails created by moving objects underwater. These new insights into the biological foundation of tactile perception through whiskers provide new design criteria for developing efficient underwater robotic sensors.

## 1. Introduction

The design of marine intelligent equipment, such as unmanned ships, submarines, and underwater robots, has become a popular topic in ocean exploration and transportation activities [1,2]. The accurate perception ability in complex ocean environments is the key to the safe, stable, and efficient operation of marine intelligent equipment, especially in underwater environments [3,4]. Underwater vision technology based on optics and underwater hearing technology based on ultrasound have been widely used in practical engineering. However, optics and ultrasound are also affected by many types of interference during underwater transmission [5–10]. For example, the scattering caused by underwater suspended objects leads to problems of underwater vision such as low contrast, blurred edges, and poor quality. The sound waves are susceptible to ocean noise, self-noise, target reflection characteristics, obstacles, and others, resulting in multipath effects and Doppler frequency shifts. This interference makes it difficult for underwater

intelligent equipment to work agilely in turbid and narrow areas. Therefore, there is an urgent need to develop new underwater sensing technologies for underwater intelligent equipment to enhance the ability to perceive the surrounding environment.

As a new sensing form for the underwater environment, tactile perception can provide environmental information for underwater equipment [11]. Some research groups have concentrated on underwater bionic tactile technology inspired by the abilities of underwater creatures to sense variations in the external environment [12–14]. Fish and some aquatic amphibians with lateral line systems are able to perceive small fluid movements and pressure gradient changes. Pressure sensors and micro- electromechanical systems (MEMS) technology can be used to construct artificial lateral line arrays, which can evaluate the environmental flow field by sensing variations of the pressure [15,16]. With their facial whiskers, seals can effectively perceive variations of the environmental flow field caused by external factors [17,18]. Based on the capabilities of seal whiskers, a fluid motion sensor was designed, and

some fluid properties of the seal whiskers were explored [19]. Graphene materials and piezoelectric materials can be used to design whisker sensors to sense the environmental flow field based on the deflection of the bionic whiskers [20,21]. To the best of the authors' knowledge, there has been no study combining triboelectric nanogenerators (TENGs) with seal whiskers.

TENGs based on triboelectrification and electrostatic induction have been developing as an innovative electromechanical conversion technology, providing ultra-high sensitivity to mechanical stimuli and exhibiting excellent performances in energy har- vesting and self-powered sensing [22–25]. Self-powered TENG sensors have shown responses to environmental stimulation [26,27], ultra-high sensitivity to acoustic properties [28,29], wearable devices [30–35], harvesting of ocean waves and current energy [36–38], human-computer interactions [39,40], and status monitoring [41–44]. An early study proposed a triboelectric whisker sensor based on the bionic structures of rat whiskers that could evaluate unknown environments [45,46]. TENG can be composed by the diversity of flexible materials, therefore it has excellent adaptability with supporting structures. More importantly, the TENG can produce high voltage output under minor disturbances. This makes sensors based on TENG have the advantages of self-powered and high signal-to-noise ratio. With these capabilities, a bionic tactile sensor based on TENGs could provide a novel and simple solution for the tactile sensing of underwater intelligent equipment.

Herein, we report a fully flexible, simple-structure, self-powered, free-standing channel underwater bionic whisker sensor (UBWS) for
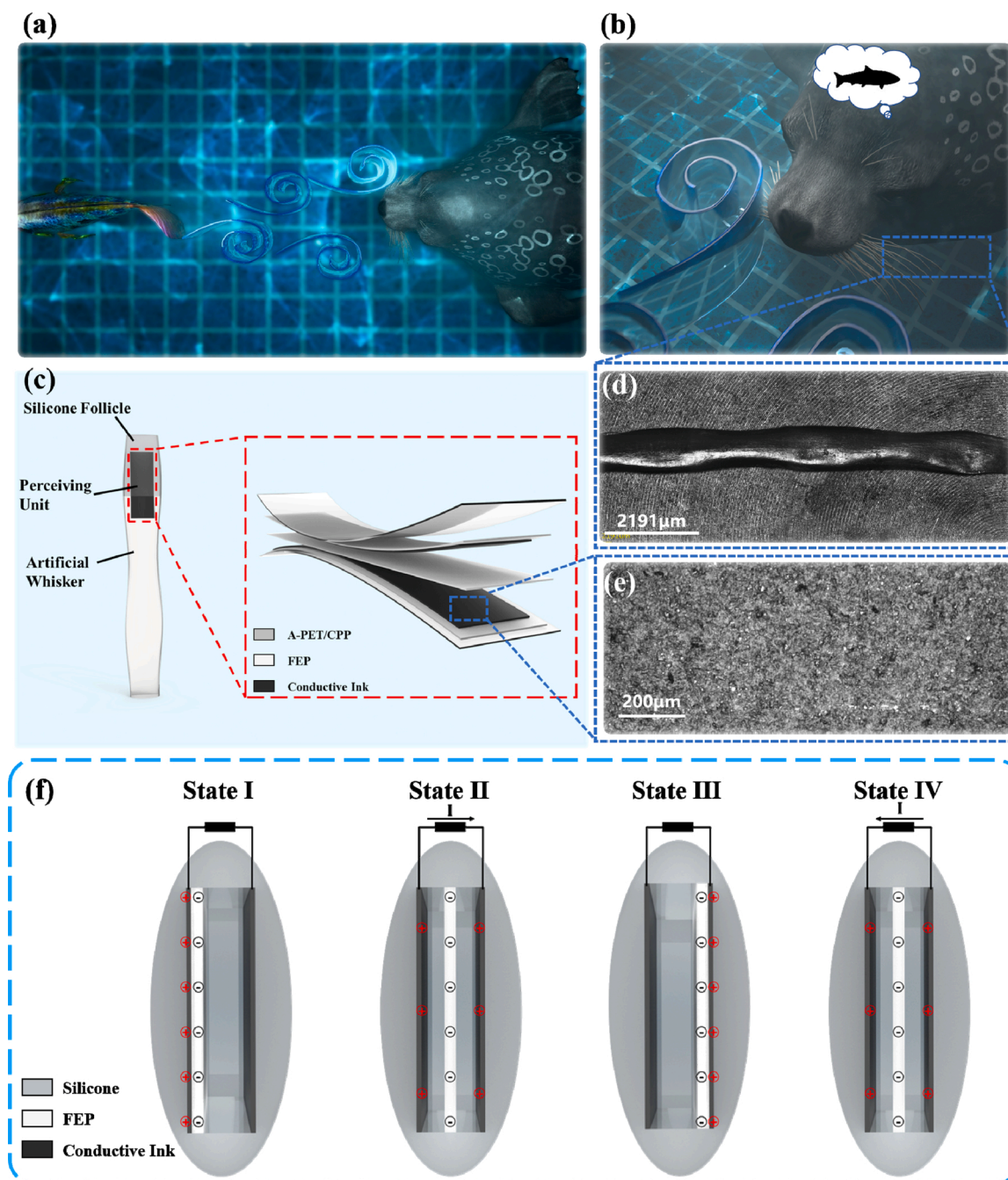


**Fig. 1.** Structure and working mechanism of underwater bionic whisker sensor (UBWS). (a) A seal tracks a moving fish underwater with its whiskers. (b) A target is perceived through the effect of the vortex on the whiskers. (c) Structural diagram of UBWS. (d) Scanning electron microscopy image of the structure of a seal whisker. (e) Scanning electron microscopy image of the conductive ink electrodes. (f) Schematic charge distribution as the fluorinated ethylene propylene (FEP) film moves.

sensing passive vortices caused by swimming targets. The UBWS is composed of an inner TENG perceiving unit, a flexible silicone follicle, and an artificial whisker. Furthermore, the perceiving unit is encapsulated with electrostatic shielding material, which improves the output performance of the UBWS underwater. The performance of the UBWS was systematically studied both theoretically and experimentally. Three motion parameters of the target affected the output performance of the UBWS, and the regular pattern suggested that the UBWS could be used to assess the motion state of the underwater target. Through theoretical analysis, a composite model of the UBWS was constructed to deeply study its perceptual capabilities. Finally, based on the perception capability of the UBWS, we realized the real-time control of external modules, monitoring of the target motion status, and tracking of underwater targets.

## 2. Results and discussion

### 2.1. Structure and working principle of underwater bionic whisker sensor

Fig. 1(a) and (b) show the schematic diagram of a swimming fish tracked by a seal, which is capable of identifying and locating prey by perceiving the change of the vortices in the flow field using its whiskers. In early studies [19], researchers found that the seal whiskers have unique wave-shaped characteristics, which assist in perception and reduce the effects of $\theta$-vortex-induced vibrations by seal's own motion. The detailed scanning electron microscopy photograph of the whisker is shown in Fig. 1(d). Based on this structure, an underwater bionic whisker sensor was designed to sense underwater vortices from a moving target passively. As shown in Fig. 1(c), the structure of the UBWS was mainly composed of an inner TENG perceiving unit, a flexible silicone follicle (Dragonskin 00–20), and an artificial whisker (polydimethylsiloxane, PDMS). The follicle wrapped the upper half of the perceiving unit, and the artificial whisker wrapped the lower half. The difference in the material elasticity be- tween the upper and lower halves caused the main deflection point of the UBWS on the perceiving unit interval. Furthermore, the perceiving unit consisted of aluminum-coated polyethylene glycol terephthalate/cast polypropylene (A-PET/CPP), fluorinated ethylene propylene (FEP), and conductive ink. It is worth noting that the FEP film and conductive ink painted on the FEP film were the dielectric layer and electrodes, respectively. Fig. 1(e) shows the scanning electron microscopy image of the conductive ink electrodes. The increased roughness of the ink surface could increase the contact area between the two materials, resulting in the improvement of the output voltage of the UBWS. Furthermore, A-PET/CPP was used as the packaging material of the perceiving unit. Due to the Faraday cage effect of the electrostatic shielding material, the performance of the UBWS only attenuated 10% in the underwater environment compared to air, as shown in Fig. S1.

Fig. 1(f) shows a generation cycle of the UBWS under short-circuit conditions. When the artificial whisker deflected, the dielectric layer contacted the electrode layer on one side, creating opposite charges on the surfaces of the two materials through a triboelectric effect. The dielectric layer had a negative charge on its surface, and the electrode layer had a positive charge due to the higher electronegativity of the FEP than that of the conductive ink. When the dielectric layer was separated from the electrode layer, a positive charge was generated at the opposite electrode due to the flow of free electrons in the external circuit from one side of the electrode layer to the other, balancing the potential difference. Affected by the pressure difference due to the vortex, the whisker continued to deflect, and the charge was completely transferred when the dielectric layer contacted the electrode layer on the other side. Thereafter, the whisker returned to its neutral position, and the charge began a round of reverse transfer, creating an opposite output signal. Fig. S2 shows the simulated potential distribution for the four states, these results were obtained in COMSOL using finite element analysis. Based on the visualization of the flow field, the detailed sensing

mechanism of the UBWS is described in Note S1.

### 2.2 Output performance of UBWS

A schematic of the experimental platform used to test the performance of the UBWS is shown in Fig. 2(a), where a rubber fishtail driven by a steering gear was used as a vortex generator, and the UBWS was set up behind the fishtail to perceive its motion state. As shown in Fig. S3, we denote the swing angle, swing frequency, and dimensionless number distance as $\theta$, $f$, and $D/L$, respectively. Here, $D$ is the distance between the fishtail and the UBWS, and $L$ is the characteristic length of the UBWS. For $\theta = 54deg$ and $f = 2Hz$, Fig. 2(b) shows the influence of $D/L$ on the output voltage of the UBWS. As $D/L$ gradually increased from 1 to 5, the peak output voltage increasingly decreased. This was because the pressure differential caused by the vortex gradually dissipated as the distance between the device and vortex increased. In addition, a leave-one-out cross-validation (LOOCV) strategy was used to fit the $D/L - U$ model, and the detection accuracies and generalization performances of these models are shown in Fig. 2(c). This confirmed that the linear model had a high correlation coefficient of 0.99459 at all $D/L$ values, with errors less than 3.2%.

Fig. 2(d) shows the influence of the swing angle on the output voltage of the UBWS for $D/L = 1$ and $f = 2Hz$. As the $\theta$ increased from 18 to 90 $deg$, the output voltage increased continually, but the trend gradually slowed. The detection accuracy and generalization of the $\theta - U$ model when using the LOOCV strategy are shown in Fig. 2(e). The output voltage also fits well with a quadratic function of the swing angle with a high correlation coefficient of 0.99815. To further illustrate the effects of $D/L$ and the swing angle on the output, Fig. 2(f) shows the relationships between them. The two parameters had different effects on the output voltage signal of the UBWS, which indicated that the swing angle had a greater influence on the generated output voltage. The effects of the different electrode and dielectric layer materials on the output voltage of the UBWS are shown in Fig. S4.

To investigate the effect of the swing frequency on the output, a vibration dynamics model is described by the Euler–Bernoulli undamped beam model with a uniform cross-section, as shown in Fig. S6(a). Based on the model analysis and a simulation, the natural resonant frequency of the UBWS was around 2 $Hz$, meaning that the whisker could reach the best deflection state when the swing frequency of the fishtail was near 2 $Hz$, which is shown in Fig. S6(b) and S6(c). For $D/L = 1$ and $\theta = 54deg$, Fig. 2(g) shows that the output voltage of the UBWS reached a peak value when the swing frequency was close to the resonance frequency. The detection accuracy and generalization ability of the $f - U$ model are shown in Fig. 2(h), indicating that the output voltage was fit well by a quadratic function of the swing frequency with a high correlation coefficient of 0.99276. Under the condition of $D/L = 1$, the relation- ship between the output voltage of the UBWS, swing frequency, and swing angle is shown in Fig. 2(i). Fig. S7(e) and S7(f) clearly illustrate the relationships between $f$, $D/L$, $\theta$, and the output voltage of the UBWS for $\theta = 54deg$ and $D/L = 1$. For $D/L = 2$–5, the influence of the swing angle on the output voltage of the UBWS is shown in Fig. S7, proving the generality of the above results. The durability testing results of the UBWS are shown in Fig. S5. The output performance remained in a good state even after 30 days. The directional experimental results of the UBWS are shown in Fig. S8, indicating that the UBWS had a certain ability to resolve vortices in different directions. And the output performance of the UBWS when the relevant parameters of water quality changed is shown in Fig. S11. Therefore, the proposal of the UBWS provides a novel and low-cost technical scheme for passive vortex perception.

### 2.3 Scaling law of UBWS

To study the perception mechanism of the UBWS in detail, models were used to quantify the vortices, which ultimately constituted the
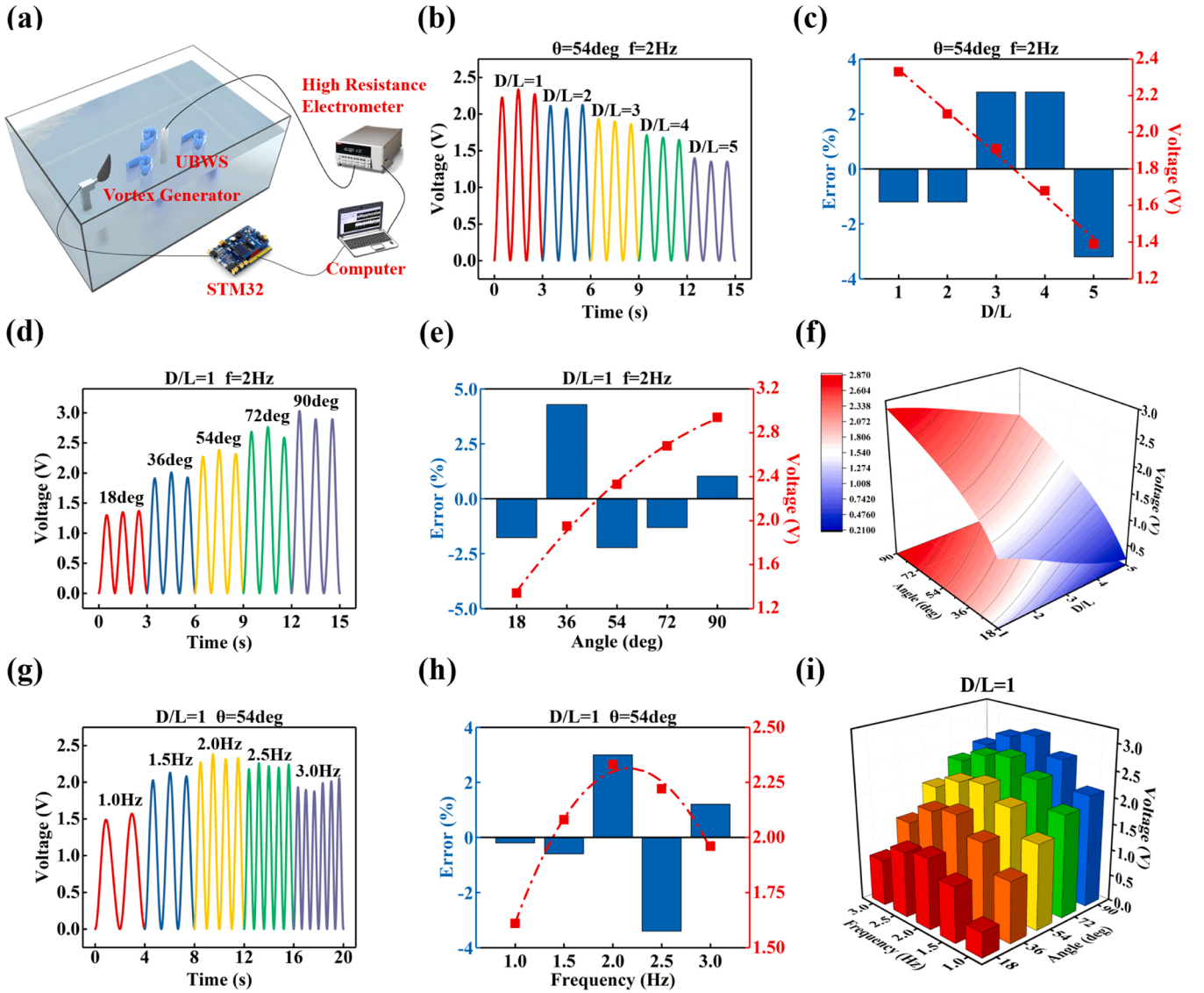
**Fig. 2.** The output performance of UBWS. (a) Schematic of the experimental setup used. (b) Response performance for $D/L = 1$–5 when $\theta = 54deg$ and $f = 2Hz$. (c) Leave-one-out cross-validation (LOOCV) for evaluating accuracy and generalization performance of the $D/L - V$ model. (d) Response performance from $\theta = 18$ to $90$ $deg$ when $D/L = 1$ and $f = 2Hz$. (e) LOOCV validation for evaluating accuracy and generalization performance of the $\theta - V$ model. (f) Relationship between the output voltage of the UBWS, distance, and swing angle. (g) Response performance for $f = 1Hz$ to $5Hz$ when $\theta = 54deg$ and $D/L = 1$. (h) LOOCV validation for evaluating accuracy and generalization performance of the $f - V$ model. (i) Relationship between the output voltage of the UBWS, swing frequency, and swing angle.

perception model of the UBWS. A schematic of the process of fishtail swinging to produce an anti-*Karman* vortex is shown in Fig. 3(a). According to the detailed theory [47–50] in Note S2, the vortex strength Γ can be expressed as

$$\Gamma = \alpha Afc = \alpha fc^2 sin\frac{\theta}{2} \#\tag{1}$$

ere $\alpha$ is a proportionality factor, and $c$ is the chord length of the fishtail. As shown in Fig. 3(b), the vortex strength was affected by both the swing angle and frequency, and the increase in the angle and frequency would lead to an increase in the vortex strength. The vortex width h can be expressed as

$$h = \beta A = \beta csin\frac{\theta}{2}\#\tag{2}$$

where $\beta$ is a proportionality factor. The relationship between the vortex width, swing angle, and swing frequency is shown in Fig. 3(c). The vortex width was fit well by a linear function of the swing angle, and the

swing frequency basically did not affect the vortex width. A model relating the vortex to the force on the bionic whisker is shown in Fig. 3 (d), where $(x_v, y_v)$ is the coordinate of the vortex center, and $(x, 0)$ is the coordinate of the stress point. When a vortex flows near the whisker, the pressure difference would cause the whisker to deflect. According to the detailed theory [51,52] in Note S2, the maximum force on the surface of the artificial whisker $F_{max}$ can be expressed as

$$F_{max} = \frac{1}{2\pi}\bullet\frac{1}{L_a}b\rho_f\Gamma\int_0^{L_a}\left\{\frac{u_v}{\sqrt{(x-x_v)^2+(y_v)^2}} - \frac{\Gamma}{4\pi\left[(x-x_v)^2+(y_v)^2\right]}\right\}\bullet xdx\#$$

$$\tag{3}$$

where $L_a$ is the width of the artificial whisker, $b$ is the length of the whisker, $\rho_f$ is the density of the fluid, and $u_v$ is the velocity of the vortex in the x-direction. Fig. 3(e) shows the influence of the vortex strength and width on the maximum force on the artificial whisker. When the vortex width was constant, the maximum force increased with the increase in the vortex strength. When the vortex strength was constant, the
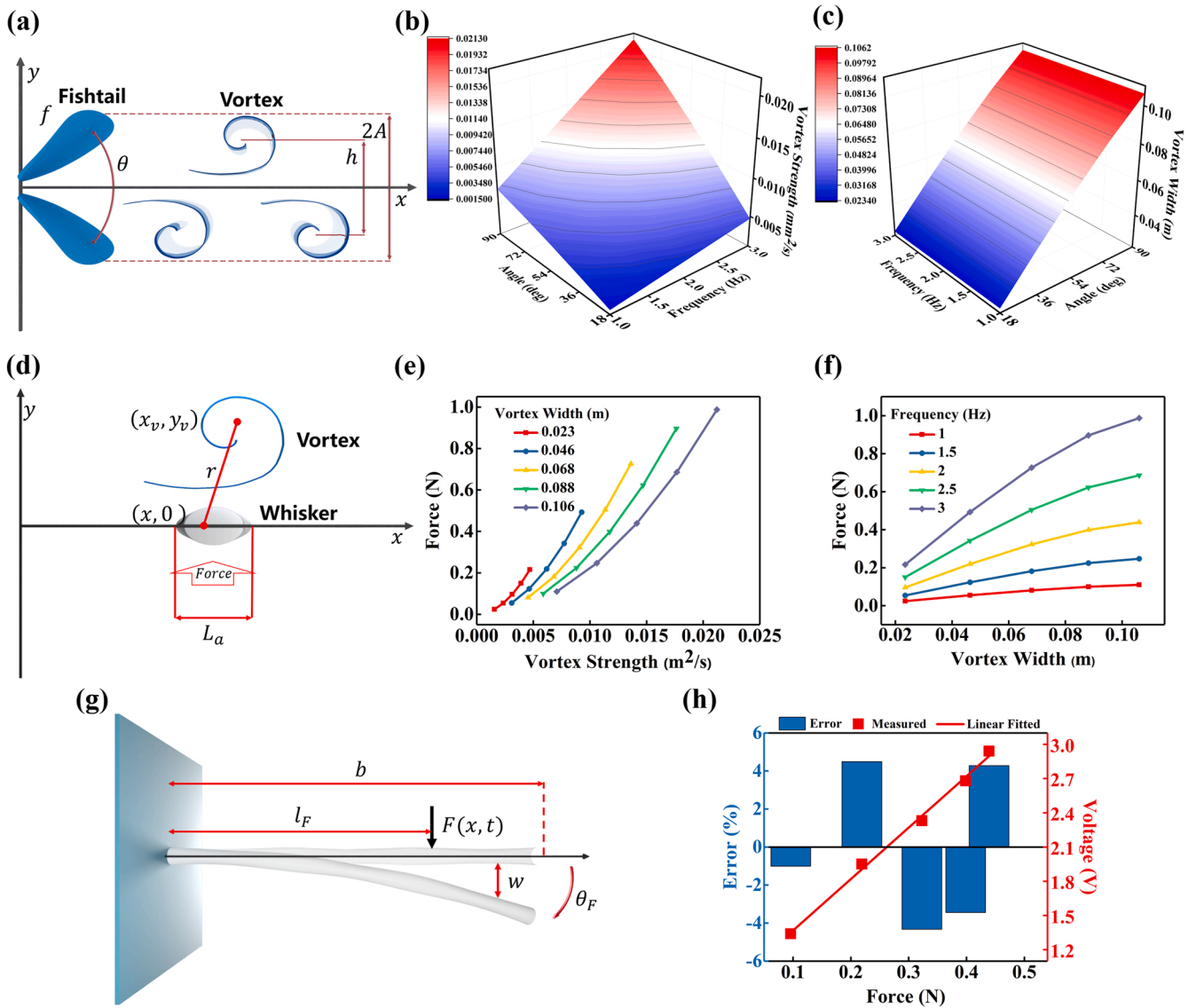
**Fig. 3.** Theoretical models of the UBWS. (a) Schematic of the flow field behind the fishtail. (b) Relation- ship between the vortex strength, swing angle, and swing frequency. (c) Relationship between the vortex width, swing angle, and swing frequency. (d) Schematic of the force on the whisker exerted by the vortex. (e) Influence of the vortex strength on the surface force of the whisker under different vortex widths. (f) Influence of the vortex width on the surface force of the whisker under different vortex frequencies. (g) Schematic of the deflection of the whisker by a force. (h) Theoretical value of the output voltage of the UBWS and the actual measured value under different forces.

maximum force decreased with the increase in the vortex width. Fig. 3(f) shows the influence of the vortex width and the swing frequency of the fishtail on the maximum force on the artificial whisker. Here note that the maximum force kept increasing when the swing frequency increased, but a greater force did not mean that the whisker would produce greater deflection. The deflection state of the whisker was still dominated by its resonance frequency.

Finally, a more detailed model of the deflection of the artificial whisker is shown in Fig. 3(g), where the Euler–Bernoulli undamped whisker model with a uniform cross-section can be expressed as [53]

$$EI\partial^4 w / \partial x^4 + \rho A \partial^2 w / \partial t^2 = F(x,t) \#\qquad(4)$$

where $w$ denotes the whisker's lateral displacement, $x$ is the whisker's axial location, and $F(x,t)$ is the external load at time $t$. As shown in Fig. 3 (h), when $f = 2Hz$, the correlation between the experimentally measured value and the linear fit value reached 0.99411, which confirmed that UBWS realized the perception of underwater targets by sensing vortices.

## 3. Demonstration of UBWS

### 3.1 Application of UBWS in real-time control

Fig. 4(a) shows a photograph of the experimental electronic setup, with an Arduino Uno R3 used as a circuit board to perform signal sampling and data processing. The number of light-emitting diodes (LEDs) illuminated represented the relative distance between the underwater target and the UBWS. A panoramic view of the experimental setup is shown in Fig. 4(b), in which the UBWS and the vortex generator were installed on two optical plates, and the distance between them could be changed. The performance of UBWS under the influence of waves noise under the condition of $D/L = 1$, $f = 2Hz$ and $\theta = 54deg$ is shown in Fig. S12, and the signal-to-noise ratio is about 19 dB without filtering. The corresponding circuit is depicted in Fig. 4(c). When the vortex from the motion of the underwater target was captured by the UBWS, an output voltage signal was generated. The UBWS controlled the on/off state of the LED lights by a threshold strategy (see Supplementary Movie S2). When the output voltage of the UBWS was in the
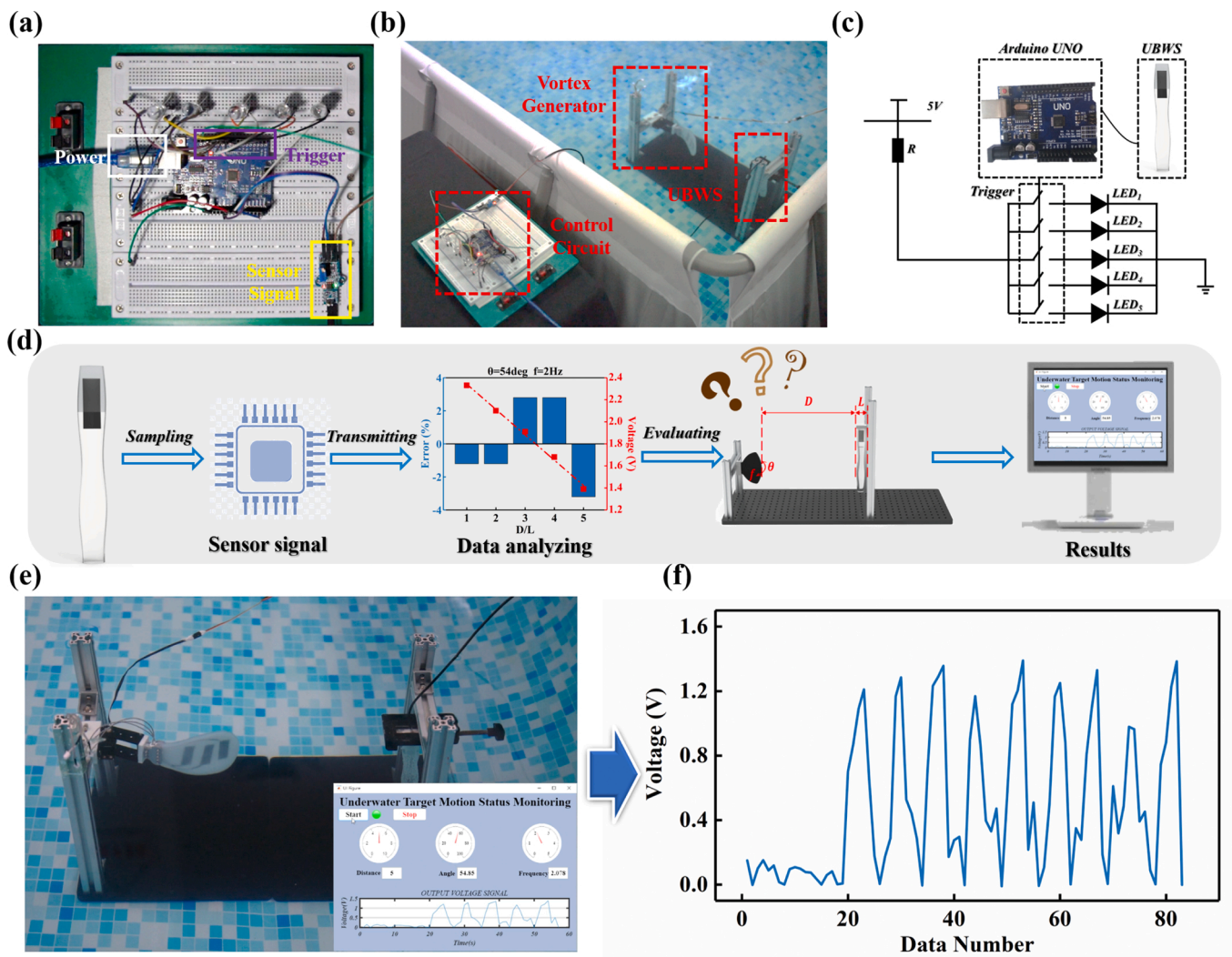
**Fig. 4.** Application of UBWS in real-time control and target motion status monitoring. (a) Schematic of the experimental electronic setup. (b) Schematic of the experimental setup. (c) Electronic module used for controlling light-emitting diode (LED) lights. (d) Logical block diagram showing how the UBWS achieved target motion state monitoring. (e) Schematic of the visualization interface and experimental setup. (f) Data collected by Arduino.

preset signal interval, the designed control strategy identified the relative distance between the underwater target and the UBWS corresponding to this interval, and the corresponding switch value to light up the LED was output by the Arduino. The results proved that the UBWS had real-time control abilities.

Supplementary material related to this article can be found online at doi:10.1016/j.nanoen.2022.107210.

### 3.2 Application of UBWS in target motion status monitoring

For further verification of the UBWS's ability to monitor the movement state of the underwater target, a visualization interface based on MATLAB was designed to display the motion parameters of the target in real time (see Supplementary Movie S3). Fig. 4(d) shows the logical block diagram of how the UBWS achieved target motion state monitoring. The Arduino received the output voltage of the UBWS, combined the previous fitting model for data processing, and converted it to the motion parameters of the target. An image of the visualization interface and the experimental setup is shown in Fig. 4(e). The UBWS was fixed on an optical plate while a swing fishtail driven by a steering gear was used as a swimming underwater target. Fig. 4(f) shows the data collected by the Arduino through the acquisition module. The frequency information was obtained from the period of the output voltage, and the angle information was obtained from the output voltage amplitude combined

with the fitting model. The distance parameter was set as a constant value here because a single UBWS could not distinguish whether the main influencing parameter was the distance or the angle when the swimming target was relatively stationary. In the future, this function can be realized by building a UBWS array. This demonstration shows the feasibility of using the UBWS for constructing an electronic reactive target motion status monitor with a low cost based on vortex sensing.

Supplementary material related to this article can be found online at doi:10.1016/j.nanoen.2022.107210.

### 3.3 Application of UBWS in target tracking

To explore the compatibility of the UBWS with marine intelligent equipment, an independently designed robotic fish integrated with the UBWS was prepared to perform underwater target tracking. An indoor water pool (3 m × 2 m × 1.5 m) was used to house the experimental setup, as shown in Fig. 5(a). The UBWS was connected to the Arduino control module in the robotic fish via an acquisition module. Subsequently, a simple closed-loop control system was built for tracking underwater targets. Fig. 5(b)–(d) shows three states during the movement of the robotic fish. Fig. 5(e) shows the corresponding voltage signal (see Supplementary Movie S4). When the UBWS captured the vortex information of the underwater target, the robotic fish moved in the direction toward the target until the voltage signal reached the set threshold. Due
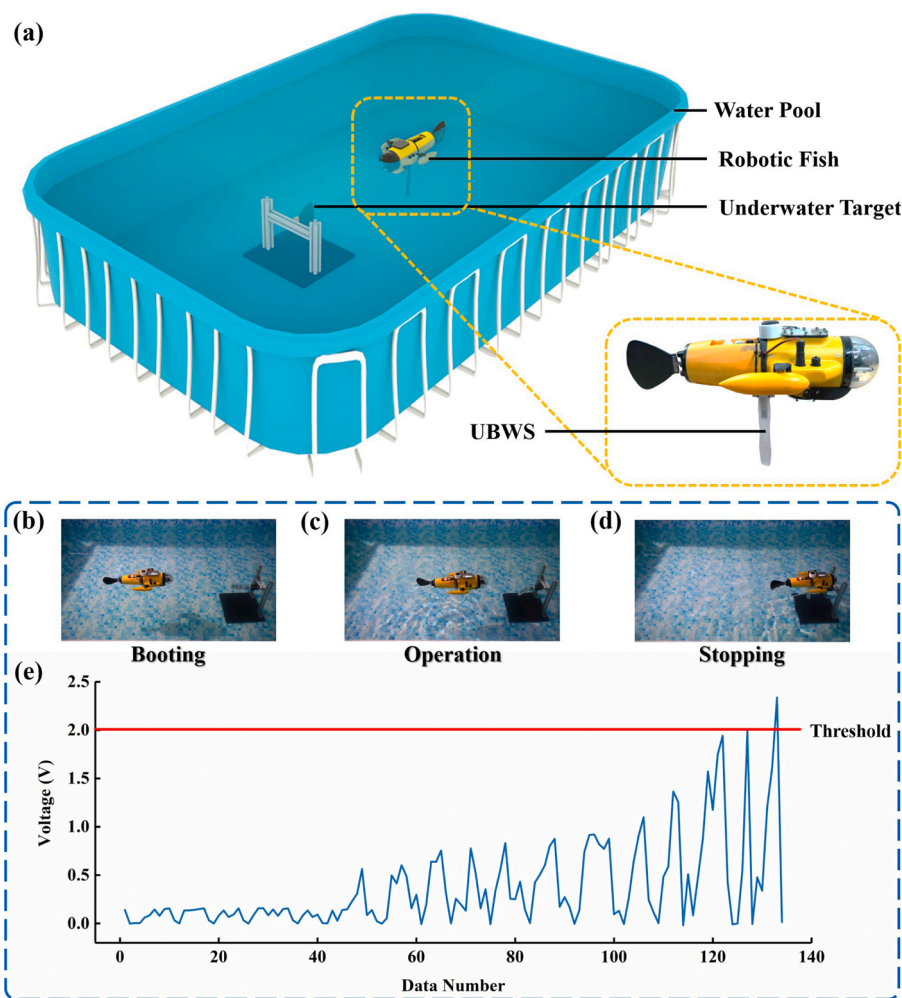
**Fig. 5.** Application of UBWS in target tracking. (a) Schematic of the experimental setup. (b)–(d) Three states during the movement of the robotic fish. (e) Corresponding voltage signal of the UBWS.

to the delay of the data transmission and the inertia of its own motion, the robotic fish could not brake in time. Therefore, the underwater target could be tracked when visual cues were reduced or absent, verifying the feasibility of applying the UBWS to marine intelligent equipment.

Supplementary material related to this article can be found online at doi:10.1016/j.nanoen.2022.107210.

## 4. Conclusion

In this study, an underwater bionic whisker sensor (UBWS) based on triboelectric nanogenerators was designed, which could be used as a supplement to the perception system of marine intelligent equipment. To demonstrate the structure, bionic principle, and sensing principle of the UBWS, the variation trends of the UBWS output when passively sensing a vortex under the disturbance of an underwater target were presented. In the case of different motion parameters, the output peak showed a good correlation trend that supported the accurate measurement of the motion information. The design of the UBWS herein advances our ability to replicate the seal's remarkable mechanoreceptive sensory abilities. In addition, the UBWS possessed the ability to dynamically capture this effect. The UBWS combined with threshold logic could be used to control external modules in real-time as a preliminary attempt to integrate with intelligent equipment. In addition, the UBWS could be combined with a host computer program to monitor the motion state of the underwater target. Moreover, we integrated the UBWS into a robotic fish to track the underwater target, illustrating the potential application value of the UBWS for passive vortex perception.

## 5. Materials and methods

### 5.1 Fabrication of UBWS

The artificial whisker was made of the SYLGARD 184 silicone elastomer. Specifically, 50 ml of solution base and 5 ml of solution agent were mixed in a 10:1 vol ratio and then stirred with an electric stirrer at 100 rpm for 3–4 min. A vacuum pump was used to vacuum the mixture to − 0.1 MPa for 2 min before the mixture was poured into a 3D-printed resin mold and cooled at 20 ℃ for 24 h. This process yielded an artificial whisker with a length of 150 mm. Two 0.3-mm-thick FEP films printed with conductive ink were cut into pieces with dimensions of $12 \times 4$ mm$^2$ to form electrodes, and a 0.3-mm-thick FEP film was cut into pieces with dimensions of $12 \times 42$ mm$^2$ to form a dielectric layer. These sections were encapsulated by a 0.15-mm-thick A-PET/CPP film. The induced voltage was transmitted by 0.3-mm-thick copper wires attached to the electrodes. This process yielded a perceiving unit with $15 \times 45$ mm$^2$, and the perceiving unit was installed into the grooves of the whisker. Similarly, a flexible silicone follicle was made of Dragonskin 00–20 silica gel with a 1:1 vol ratio and the same treatment as that used for the SYLGARD 184. The assembled perceiving unit and whisker were placed in a new 3D-printed resin mold, and the vacuumed silica gel mixture was poured into the mold and cooled at 25 ℃ for 36 h.

A bionic tactile sensor was finished with a length of 200 mm.

*5.2 Electric measurement and characterization*

The UBWS was mounted vertically to a fixture adapter that was installed on a platform constructed from aluminum profiles (TDT-3030) and optical panels ($300 \times 300 \times 13$ mm$^3$). At different frequencies and swing angles, a vortex generator was used to generate vortices for different conditions, which was formed by a rubber fishtail driven by a digital servo. The digital servo was controlled by an STM32F103R8 chip. The signal produced by the UBWS was measured with a Keithley 6514 electrometer, and the measurement was displayed in a custom LabVIEW VI application. A photograph of the experimental setup is shown in Fig. S3.

**CRediT authorship contribution statement**

**Siyuan Wang:** Investigation, Methodology, Software, Data curation and Writing – review. **Peng Xu:** Conceptualization, Software, Writing – review & editing. **Xinyu Wang:** Data curation, Software. **Jiaxi Zheng:** Investigation and Software. **Xiangyu Liu:** Data curation. **Jianhua Liu:** Investigation and Visualization. **Tianyu Chen:** Software. **Hao Wang:** Data curation. **Guangming Xie:** Conceptualization, Methodology. **Jin Tao:** Conceptualization, Methodology, Writing – review & editing. **Minyi Xu:** Conceptualization, Methodology, Writing – review & editing.

*Conflict of Interest*

The authors declare no conflict of interest.

**Appendix A. Supporting information**

Supplementary data associated with this article can be found in the online version at doi:10.1016/j.nanoen.2022.107210.

**References**

[1] M. Lin, C. Yang, Ocean observation technologies: a review, Chin. J. Mech. Eng. 33 (1) (2020) 1–18.
[2] G. Li, X. Chen, F. Zhou, Y. Liang, Y. Xiao, X. Cao, Z. Zhang, M. Zhang, B. Wu, S. Yin, et al., Self-powered soft robot in the mariana trench, Nature 591 (7848) (2021) 66–71.
[3] M.R. Arshad, Recent advancement in sensor technology for underwater applications, Indian, J. Geo-Mar. Sci. (IJMS) 38 (2009) 267–273.
[4] M. Krieg, K. Nelson, K. Mohseni, Distributed sensing for fluid disturbance compensation and motion control of intelligent robots, Nat. Mach. Intell. 1 (5) (2019) 216–224.
[5] M. Jian, X. Liu, H. Luo, X. Lu, H. Yu, J. Dong, Underwater image processing and analysis: a review, Signal Process.: Image Commun. 91 (2021), 116088.
[6] F. Hidalgo, T. Bräunl, Review of underwater slam techniques, in: 2015 6th International Conference on Automation, Robotics and Applications (ICARA), IEEE, 2015, pp. 306–311.
[7] K.M. Awan, P.A. Shah, K. Iqbal, S. Gillani, W. Ahmad, Y. Nam, Underwater wireless sensor networks: a review of recent issues and challenges, Wirel. Commun. Mob. Comput. 2019 (2019) 6470359.
[8] J. W.. YAM, 2021.Investigation on the effects and performance of underwater imaging target detection, Ph.D. thesis, Monash University (2021).
[9] Y. Zhang, B. Qin, G. Zhu, G. Gao, L. Luo, W. Chen, Effect of sediment resuspension on underwater light field in shallow lakes in the middle and lower reaches of the yangtze river: a case study in longgan lake and taihu lake, Sci. China Ser. D. 49 (1) (2006) 114–125.
[10] K. Sun, W. Cui, C. Chen, Review of underwater sensing technologies and applications, Sensors 21 (23) (2021) 7849.
[11] Y. Liu, R. Bao, J. Tao, J. Li, M. Dong, C. Pan, Recent progress in tactile sensors and their applications in intelligent systems, Sci. Bull. 65 (1) (2020) 70–88.
[12] C. Jiang, Q. Li, N. Sun, J. Huang, R. Ji, S. Bi, Q. Guo, J. Song, A high- performance bionic pressure memory device based on piezo-oled and piezo- memristor as luminescence-fish neuromorphic tactile system, Nano Energy 77 (2020), 105120.
[13] J. Zhang, Z. Ma, S. Li, L. Pan, Y. Shi, Recent research progress in biomimetic tactile sensors, Sci. Sin. Technol. 50 (1) (2019) 1–16.
[14] Y. Zou, P. Tan, B. Shi, H. Ouyang, D. Jiang, Z. Liu, H. Li, M. Yu, C. Wang, X. Qu, et al., A bionic stretchable nanogenerator for underwater sensing and energy harvesting, Nat. Commun. 10 (1) (2019) 1–10.
[15] Y. Yang, N. Nguyen, N. Chen, M. Lockwood, C. Tucker, H. Hu, H. Bleckmann, C. Liu, D.L. Jones, Artificial lateral line with biomimetic neuromasts to emulate fish sensing, Bioinspir. Biomim. 5 (1) (2010), 016001.
[16] Y. Jiang, Z. Ma, D. Zhang, Flow field perception based on the fish lateral line system, Bioinspir. Biomim. 14 (4) (2019), 041001.
[17] W. Hanke, M. Witte, L. Miersch, M. Brede, J. Oeffner, M. Michael, F. Hanke, A. Leder, G. Dehnhardt, Harbor seal vibrissa morphology suppresses vortex- induced vibrations, J. Exp. Biol. 213 (15) (2010) 2665–2672.
[18] H. Hans, J. Miao, M. Triantafyllou, Mechanical characteristics of harbor seal (Phoca vitulina) vibrissae under different circumstances and their implications on its sensing methodology, Bioinspir. Biomim. 9 (3) (2014), 036013.
[19] H.R. Beem, 2015. Passive wake detection using seal whisker-inspired sensing, Tech. rep., Massachusetts Inst of Tech Woods Hole Ma Dept of Applied Ocean Physics and Engineering (2015).
[20] J.Z. Gul, K.Y. Su, K.H. Choi, Fully 3d printed multi-material soft bio- inspired whisker sensor for underwater-induced vortex detection, Soft Robot. 5 (2) (2018) 122–132.
[21] P.V. y Alvarado, V. Subramaniam, M. Triantafyllou, 2012. Design of a bio-inspired whisker sensor for underwater applications, SENSORS, 2012 IEEE(2012) pp. 1–4.
[22] M. Willatzen, Z.L. Wang, Theory of contact electrification: Optical transitions in two-level systems, Nano Energy 52 (2018) 517–523.
[23] Z.L. Wang, On maxwell's displacement current for energy and sensors: the origin of nanogenerators, Mater. Today 20 (2) (2017) 74–82.
[24] W.-G. Kim, D.-W. Kim, I.-W. Tcho, J.-K. Kim, M.-S. Kim, Y.-K. Choi, Tribo- electric nanogenerator: structure, mechanism, and applications, ACS Nano 15 (1) (2021) 258–287.
[25] Z.L. Wang, T. Jiang, L. Xu, Toward the blue energy dream by triboelectric nanogenerator networks, Nano Energy 39 (2017) 9–23.
[26] M. Xu, P. Wang, Y.-C. Wang, S.L. Zhang, A.C. Wang, C. Zhang, Z. Wang, X. Pan, Z. L. Wang, A soft and robust spring based triboelectric nanogenerator for harvesting arbitrary directional vibration energy and self-powered vibration sensing, Adv. Energy Materials 8 (9) (2018) 1702432.
[27] X. Xiao, X. Zhang, S. Wang, H. Ouyang, P. Chen, L. Song, H. Yuan, Y. Ji, P. Wang, Z. Li, et al., Honeycomb structure inspired triboelectric nanogenerator for highly effective vibration energy harvesting and self-powered engine condition monitoring, Adv. Energy Mater. 9 (40) (2019) 1902460.
[28] H. Guo, X. Pu, J. Chen, Y. Meng, M.-H. Yeh, G. Liu, Q. Tang, B. Chen, D. Liu, S. Qi, et al., A highly sensitive, self-powered triboelectric auditory sensor for social robotics and hearing aids, Sci. Robot. 3 (20) (2018) eaat2516.
[29] H. Zhao, X. Xiao, P. Xu, T. Zhao, L. Song, X. Pan, J. Mi, M. Xu, Z.L. Wang, Dual-tube helmholtz resonator-based triboelectric nanogenerator for highly efficient harvesting of acoustic energy, Adv. Energy Mater. 9 (46) (2019) 1902824.
[30] K. He, Y. Liu, M. Wang, G. Chen, Y. Jiang, J. Yu, C. Wan, D. Qi, M. Xiao, W.R. Leow, et al., An artificial somatic reflex arc, Adv. Mater. 32 (4) (2020) 1905399.
[31] Y. Qiu, Y. Tian, S. Sun, J. Hu, Y. Wang, Z. Zhang, A. Liu, H. Cheng, W. Gao, W. Zhang, et al., Bioinspired, multifunctional dual-mode pressure sensors as electronic skin for decoding complex loading processes and human motions, Nano Energy 78 (2020), 105337.
[32] Y. Qiu, C. Wang, X. Lu, H. Wu, X. Ma, J. Hu, H. Qi, Y. Tian, Z. Zhang, G. Bao, et al., A biomimetic Drosera capensis with adaptive decision-predation behavior based on multifunctional sensing and fast actuating capability, Adv. Funct. Mater. (2021) 2110296.
[33] Y. Qiu, S. Sun, C. Xu, Y. Wang, Y. Tian, A. Liu, X. Hou, H. Chai, Z. Zhang, H. Wu, The frequency-response behaviour of flexible piezoelectric devices for detecting the magnitude and loading rate of stimuli, J. Mater. Chem. C. 9 (2) (2021) 584–594.
[34] Z. Liu, G. Wang, C. Ye, H. Sun, W. Pei, C. Wei, W. Dai, Z. Dou, Q. Sun, C.-T. Lin, et al., An ultrasensitive contact lens sensor based on self-assembly graphene for continuous intraocular pressure monitoring, Adv. Funct. Mater. 31 (29) (2021) 2010991.
[35] C. Liu, Y. Wang, N. Zhang, X. Yang, Z. Wang, L. Zhao, W. Yang, L. Dong, L. Che, G. Wang, et al., A self-powered and high sensitivity acceleration sensor with vqa model based on triboelectric nanogenerators (tengs), Nano Energy 67 (2020), 104228.
[36] M. Xu, T. Zhao, C. Wang, S.L. Zhang, Z. Li, X. Pan, Z.L. Wang, High power density tower-like triboelectric nanogenerator for harvesting arbitrary directional water wave energy, ACS Nano 13 (2) (2019) 1932–1939.
[37] H. Wang, Z. Fan, T. Zhao, J. Dong, S. Wang, Y. Wang, X. Xiao, C. Liu, X. Pan, Y. Zhao, et al., Sandwich-like triboelectric nanogenerators integrated self- powered buoy for navigation safety, Nano Energy 84 (2021), 105920.
[38] S.L. Zhang, M. Xu, C. Zhang, Y.-C. Wang, H. Zou, X. He, Z. Wang, Z.L. Wang, Rationally designed sea snake structure based triboelectric nanogenerators for effectively and efficiently harvesting ocean wave energy with minimized water screening effect, Nano Energy 48 (2018) 421–429.
[39] X. Zhang, M. Yu, Z. Ma, H. Ouyang, Y. Zou, S.L. Zhang, H. Niu, X. Pan, M. Xu, Z. Li, et al., Self-powered distributed water level sensors based on liquid– solid

triboelectric nanogenerators for ship draft detecting, Adv. Funct. Mater. 29 (41) (2019) 1900327.

[40] Z.L. Wang, Triboelectric nanogenerators as new energy technology and self-powered sensors–principles, problems and perspectives, Faraday Discuss. 176 (2015) 447–458.

[41] S. Wang, Y. Wang, D. Liu, Z. Zhang, W. Li, C. Liu, T. Du, X. Xiao, L. Song, H. Pang, et al., A robust and self-powered tilt sensor based on annular liquid- solid interfacing triboelectric nanogenerator for ship attitude sensing, Sens. Actuators A: Phys. 317 (2021) 112459.

[42] M. Xu, S. Wang, S.L. Zhang, W. Ding, P.T. Kien, C. Wang, Z. Li, X. Pan, Z.L. Wang, A highly-sensitive wave sensor based on liquid-solid interfacing triboelectric nanogenerator for smart marine equipment, Nano Energy 57 (2019) 574–580.

[43] S. Wang, P. Xu, X. Wang, H. Wang, C. Liu, L. Song, G. Xie, M. Xu, 2021. Bionic tactile sensor based on triboelectric nanogenerator for motion perception, in: 2021 IEEE 16th International Conference on Nano/Micro Engineered and Molecular Systems (NEMS), IEEE, 2021, pp. 1853–1857.

[44] X. Wang, J. Liu, S. Wang, J. Zheng, T. Guan, X. Liu, T. Wang, T. Chen, H. Wang, G. Xie, et al., A self-powered triboelectric coral-like sensor integrated buoy for irregular and ultra-low frequency ocean wave monitoring, Adv. Mater. Technol. (2021) 2101098.

[45] P. Xu, X. Wang, S. Wang, T. Chen, J. Liu, J. Zheng, W. Li, M. Xu, J. Tao, G. Xie, A triboelectric-based artificial whisker for reactive obstacle avoidance and local mapping, Research 2021 (2021) 9864967.

[46] X. Wang, P. Xu, Z. Ma, S. Wang, G. Xie, M. Xu, 2020. A bio-inspired whisker sensor based on triboelectric nanogenerators, in: 2020 35th Youth Academic Annual Conference of Chinese Association of Automation (YAC), IEEE, 2020, pp. 105– 109.

[47] M.J. David, M. Mathur, R. Govardhan, J. Arakeri, The kinematic genesis of vortex formation due to finite rotation of a plate in still fluid, J. Fluid Mech. 839 (2018) 489–524.

[48] J.J. Videler, Fish Swimming, Springer Science & Business Media, 1993.

[49] G.K. Taylor, R.L. Nudds, A.L. Thomas, Flying and swimming animals cruise at a strouhal number tuned for high power efficiency, Nature 425 (6959) (2003) 707–711.

[50] Y.-L. Yu, K.-J. Huang, Scaling law of fish undulatory propulsion, Phys. Fluids 33 (6) (2021) 061905.

[51] P.G. Saffman, Vortex Dynamics, Cambridge University Press, 1995.

[52] X. Shan, R. Song, B. Liu, T. Xie, Novel energy harvesting: A macro fiber composite piezoelectric energy harvester in the water vortex, Ceram. Int. 41 (2015) S763–S767.

[53] B. Balachandran, E.B. Magrab, Vibrations, Cengage Learning, 2009.

**Xinyu Wang** is currently pursuing the master's degree in Dalian Maritime University, China. His current research interests include underwater robot tactile system and triboelectric nanogenerator.

**Jiaxi Zheng** is currently pursuing the undergraduate degree in Dalian Maritime University, China. His current research interests include Bio-Inspired Robots and Underwater Robots.

**Xiangyu Liu** is currently pursuing the master's degree in Dalian Maritime University, China. His current research interests in the self-powered system, blue energy and triboelectric nanogenerators.

**Jianhua Liu** is currently pursuing the master's degree in Dalian Maritime University, China. His current research interests include underwater robot tactile system and triboelectric nanogenerator.

**Tianyu Chen** is currently pursuing the master's degree in Dalian Maritime University, China His current research interests include flow-induced vibration, wind energy harvesting and triboelectric nanogenerator.

**Siyuan Wang** is currently pursuing his doctor degree in Dalian Maritime University, China. His current research interests in the self-powered sensing system and application, bionic sensors and triboelectric nanogenerators.

**Peng Xu** is currently pursuing his doctor degree in Dalian Maritime University, China. His current research interests include self-powered sensing system and control, bio-inspired design and control for marine and underwater robots and triboelectric nanogenerators.

**Hao Wang** received his Ph.D. degree from Texas A&M University. Now he is an associate professor in Marine engineering College, Dalian Maritime University. His research interests include motion simulation, improvement, and stability analysis of the wave energy harvester.

**Jin Tao** (Member, IEEE) received the B.Sc. degree in automation from the Qingdao University of Science and Technology, Qingdao, China, in 2008, the M.Sc. degree in control theory and control engineering from the Guangxi University of Science and Technology, Liuzhou, China, in 2011, and the Ph.D. degree in control science and engineering from Nankai University, Tianjin, China, in 2017. He is currently an Associate Professor with the College of Artificial Intelligence, Nankai University. His research interests include intelligent control, evolutionary optimization, and multiagent systems.

**Guangming Xie** (Member, IEEE) received the B.S. degree in applied mathematics and electronic and computer technology and the M.E. and Ph.D. degrees in control theory and control engineering from Tsinghua University, Beijing, China, in 1996, 1998, and 2001, respectively. He is currently a Full Professor in dynamics and control with the College of Engineering, Peking University. His research interests include smart swarm theory, multiagent systems, multirobot cooperation, biomimetic robot, switched and hybrid systems, and networked control systems.

**Minyi Xu** received his Ph.D. degree from Peking University in 2012. During 2016–2017, he joined Professor Zhong Lin Wang' group at Georgia Institute of Technology. Now he is a Professor in the Marine Engineering College, Dalian Maritime University. His current research is mainly focused on the areas of blue energy, self-powered systems, triboelectric nanogenerators and its practical applications in smart ship and ocean.